Analysis of shear-torque fatigue test for bituminous pavement interlayers

ANALYSIS OF SHEAR-TORQUE FATIGUE TEST FOR BITUMINOUS PAVEMENT INTERLAYERS

Davide Ragni[a,*], Gilda Ferrotti[a], Christophe Petit[b], Francesco Canestrari[a]

[a] *Department of Civil and Building Engineering and Architecture, Università Politecnica delle Marche, via Brecce Bianche, 60131 Ancona, Italy*

[b] *Laboratoire GC2D, Université de Limoges, Bd J. Derche, 19300 Egletons, France*

* Corresponding author.

E-mail addresses: d.ragni@pm.univpm.it (D. Ragni), g.ferrotti@univpm.it (G. Ferrotti), christophe.petit@unilim.fr (C. Petit), f.canestrari@univpm.it (F. Canestrari).

ABSTRACT

The laboratory characterisation of bituminous interlayers is a challenging issue because of the difficulty of establishing loading conditions that can simulate field behaviour. This paper describes a shear-torque fatigue test procedure aimed at investigating the fatigue behaviour of bituminous pavement interlayers. A preliminary experimental investigation, able to evaluate the damage process occurring in both single- and double-layered specimens, showed that the presence of the interface constitutes a weakness zone, noticeably influencing the shear fatigue performance of the pavement structure. Thus, a model for the description of the evolution of the interlayer damage by using the variation of the interlayer complex shear modulus was proposed and preliminarily validated. Moreover, a new fatigue failure criterion has been proposed to be used in the result analysis of the shear-torque fatigue tests.

Keywords: asphalt pavement; bituminous interlayer bonding; cyclic loading; shear-torque fatigue test; damage accumulation.

1. Introduction

It is widely recognised that interlayer bonding conditions between bituminous layers directly influence the overall pavement performance. Indeed, a proper interlayer bonding is fundamental for transferring normal and shear stresses induced by traffic loading throughout bituminous layers, providing to the pavement structure the uppermost load-bearing capacity. On the contrary, poor bonding between bituminous layers may cause low performance, which in turns could lead to slippage cracking, top-down cracking and permanent deformations [1-4], especially in the areas where the vehicles frequently accelerate, brake or turn sharply [5]. It is well known that interlayer bonding is related to a large number of factors, such as type of materials (e.g., mixture type, binder type, aggregate texture), construction characteristics (e.g., tack-coat, compaction/voids, surface roughness, contamination, reinforcement) and loading/environmental aspects (e.g., temperature, traffic speed, ageing process) [5-11] that should be taken into account during the design process.

Notwithstanding the fundamental importance of interlayer bonding condition, the pavement design methods currently lack a standardised approach to characterise interlayers. One of the main reasons is that the laboratory characterisation of bituminous interlayers is a challenging issue because of the difficulty of establishing loading conditions that can simulate field behaviour. During the last decades, several laboratory equipment has been developed to investigate the interlayer bonding based on different testing methods, loading conditions as well as specimen geometry and preparation. These tests can be classified into four main groups: tensile (pull-off), torque, wedge splitting and direct shear tests (with and without the application of normal load) [5,6,12]. Depending on the test device, these testing configurations simulate the mode of interlayer bonding failure (e.g., failure due to tensile or shear stresses) [5,6,12]. Among all, shear testing devices are the most popular test configuration for laboratory assessment of bonding condition and allow, in some cases, also the application of normal load on the interface plane to better simulate traffic loading. Typical testing protocol adopts monotonic condition in strain-controlled mode, by applying a constant displacement rate between two pavement layers until failure. It allows the determination of the interlayer shear strength (ISS), which represents

the maximum shear stress the interface can withstand before failure. Recent studies confirmed the validity of the time-temperature superposition principle for the ISS, highlighting the viscoelastic nature of such failure parameter through the adoption of sigmoidal master curves [13,14]. Notwithstanding, such a procedure entails substantial simplification of the real pavement behaviour and the ISS can only be used for quality control purposes as it does not provide any information on bonding deterioration during the pavement lifespan except in those cases where the shear stress induced by traffic is very high (i.e., where the vehicles frequently accelerate, brake or turn sharply). Thus, since the traffic loadings applied to the pavement surface are repetitive and induce progressive fatigue damage and/or accumulation of permanent deformations, it is well recognised that a quasi-static monotonic load is not appropriate to correctly simulate the traffic effect that the pavement structure undergoes during its lifetime.

This drawback can be solved by using cyclic bond tests, consisting in the repetitive application of a load or a displacement between two pavement layers, as they are expected to be able to better estimate the load-induced damage on the interlayer zone over the pavement lifetime. It has been shown [15-23] that cyclic bond testing methods can be effectively used to investigate the interlayer pavement properties even though, compared with the monotonic condition, the corresponding devices are generally more sophisticated, as well as the tests are time-consuming and require a considerable computational effort for the result analysis. Therefore, although cyclic bond tests are more effective in simulating the real mechanism experienced in-situ, very few bond test devices have been used in cyclic conditions so far. The cyclic bond tests currently available differ in terms of the working scheme, loading method (stress- or strain-controlled), testing conditions and failure criterion adopted to evaluate the fatigue life of the interlayer [15-23]. However, it is worth noting that the chosen control mode and testing conditions can have an important impact on the testing results.

In this framework, the Task Group 3 “Pavement multilayer system” of the RILEM TC 272-PIM “Phase and Interphase behaviour of bituminous Materials” carried out an interlaboratory test [15], which aimed at defining suitable test methods and deepening the understanding of the

pavement interlayer shear behaviour in terms of stiffness properties (small-strain thermo-viscoelasticity) and fatigue properties (accumulated damage).

Within this interlaboratory test, one of the participating laboratories [23] developed a new testing method, namely shear-torque fatigue test, to carry out fatigue tests on double-layered cylindrical specimens. This test allows to sophisticatedly investigate the fatigue behaviour of interlayers by applying a sinusoidal torsional load across the interface and monitor the resulting angular rotation, even if a non-uniform (i.e., linear) shear stresses distribution at the interface is obtained. In a recent study, Ragni et al. [23] showed that, during shear-torque fatigue tests, the damage (i.e., the highest permanent deformations) is mainly concentrated in the interlayer region of double-layered specimens. Therefore, it can be assumed that, for the most part, the specimen failure is due to the interface damage, which could be modelled by using the variation of the interlayer complex shear modulus.

2. Objectives

This paper presents the modelling of the behaviour of pavement bituminous interlayers during shear-torque fatigue tests, by including a preliminary validation of the model and a new fatigue failure criterion. To these purposes, three main phases have been considered as follows:

- after the description of the shear-torque fatigue test configuration, the equations for describing the material behaviour and the model of the evolution of the interlayer complex shear modulus are presented;
- shear-torque fatigue tests performed on both single- and double-layered bituminous specimens have been used for preliminary validation of the model;
- a new fatigue failure criterion has been proposed for the result analysis of the shear-torque fatigue tests, allowing the determination of the interlayer shear fatigue curve.

3. Shear-torque fatigue test procedure

In all the three phases of the investigation, a shear-torque fatigue device supplied by a servo-hydraulic testing equipment, available at the Laboratoire GC2D of the University of Limoges, has

been used to carry out the experimental program. The testing device, able to apply a torque of ±1,000 Nm and an axial load of ±100 kN, is equipped with a monitoring control system, associated with a temperature-controlled chamber.

Tests were carried out in load-controlled mode at a frequency of 10 Hz and a temperature of 20 °C. A sinusoidal torque with an amplitude T_0 and a constant axial compression load N of 0.05 kN were applied to the cylindrical specimen. A general view of the working scheme of the shear-torque fatigue test is shown in Fig. 1. In order to measure the sinusoidal torsional rotation angle, a non-contact angular sensor located on the upper steel plate was used (accuracy of 0.001°) (Fig. 1).

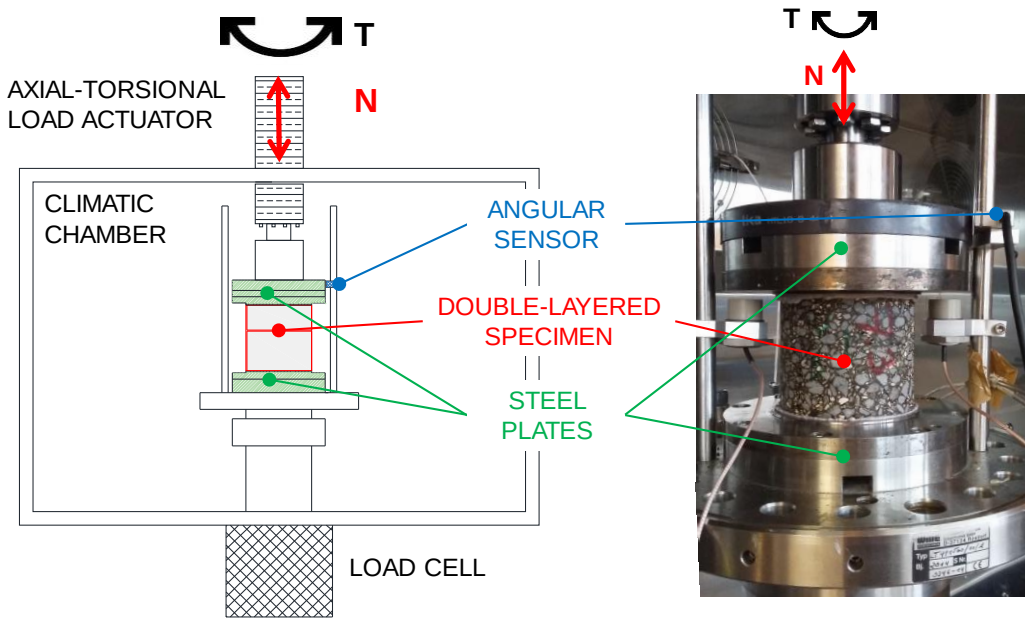

(a) (b)

Fig. 1. Shear-torque fatigue test set-up: (a) schematic view and (b) picture in the temperature-controlled chamber.

Prior to run the fatigue test, each specimen was glued with an epoxy resin to the steel plates screwed to the testing system (Fig. 1). To ensure homogeneity of the stress state in the specimen, good alignment of the specimen and steel plates is required. The specimen was conditioned at 20 °C for 4 hours and then tested.

During the test, the cyclic torque test returns a dataset which reports the evolution of torque, axial load, torsional rotation angle and phase angle as a function of the number of cycles.

Fig. 2 presents an example of experimental data for two consecutive cycles of loading at 10 Hz. Data acquisition frequency is 1,000 Hz, which gives 100 data points per cycle. Because of the great number of performed cycles, only one cycle out of 50 has been recorded.

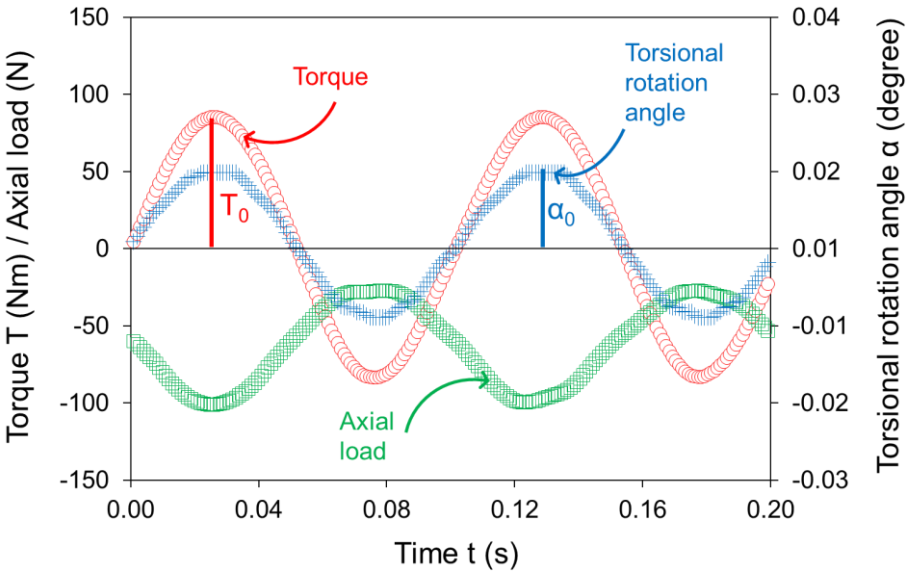

Fig. 2. Experimental data for two loading cycles at 20 °C and 10 Hz.

4. Modelling of the interface behaviour during shear-torque fatigue tests

In this phase, the evolution model of the interlayer complex shear modulus was obtained through theoretical consideration involving shear-torque fatigue test results.

4.1 Single-layered specimens

By carrying out monotonic torque tests on cylindrical specimens, it is possible to generate shear stresses that linearly increases over the radius of the specimen, as shown in Fig. 3, where $\delta(t)$ and $\gamma(t)$ are, respectively, the circumferential displacement and the shear strain over time.

The value of the maximum shear stress τ_{max} is reached on the outer circumference and can be calculated through the following equation:

$$\tau_{max} = \frac{2T}{\pi R^3} \quad (1)$$

where T is the applied torque and R is the radius of the specimen. Analogously, the maximum shear strain γ_{max}, generated by the applied torque, can be calculated as follows:

$$\gamma_{max} = \frac{\delta_{max}}{H} = \frac{R\alpha_{max}}{H} \quad (2)$$

where H is the specimen height and α_{max} is the torsional rotation angle.

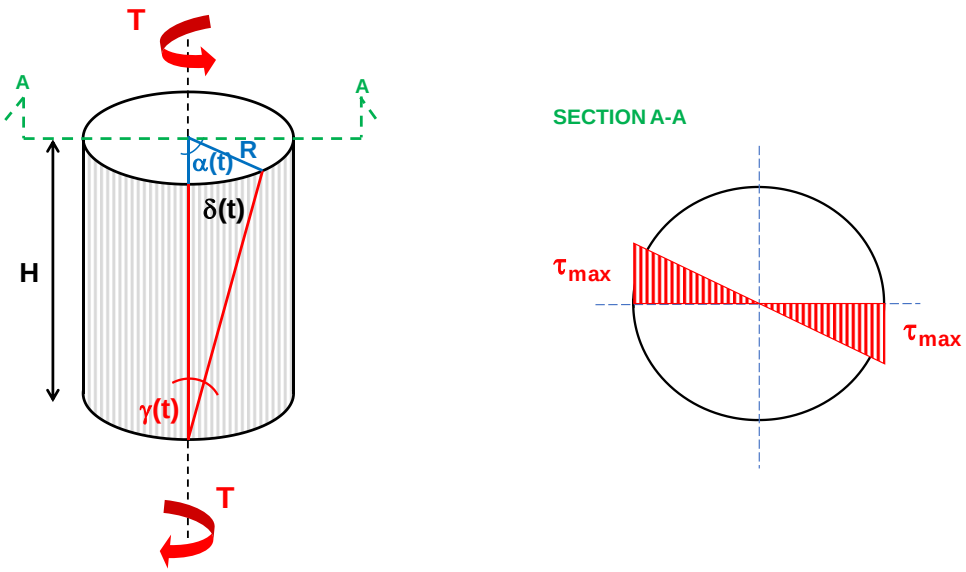

(a) (b)

Fig. 3. Schematic view of the sample (a) and its section A-A (b) subjected to shear-torque load.

When a sinusoidal loading is considered, the maximum shear stress $\tau_{max}(t)$ can be calculated as follows:

$$\tau_{max}(t) = \tau_{max,0}\sin(\omega t) = \frac{2T_0}{\pi R^3}\sin(\omega t) \quad (3)$$

where T_0 is the amplitude of the applied torque, ω is the torque pulsation ($\omega = 2\pi f$ with f the load frequency), and t is the time. The corresponding maximum shear strain $\gamma_{max}(t)$ can be obtained by using Eq. (4):

$$\gamma_{max}(t) = \gamma_{max,0}\sin(\omega t - \varphi) = \frac{R\alpha_0}{H}\sin(\omega t - \varphi) \quad (4)$$

where α_0 is the amplitude of the torsional rotation angle (Fig. 2) and φ is the phase angle, which is related to the lag between stress and strain.

The material stiffness properties have been evaluated in terms of complex shear modulus G^* of a single-layered specimen, given by the following equation:

$$G^* = \frac{\tau_{max,0}\exp[j\omega t]}{\gamma_{max,0}\exp[j(\omega t - \varphi)]} = |G^*|\exp[j\varphi] \quad (5)$$

where j is the imaginary unit (defined by $j^2 = -1$) and $|G^*|$ is the norm (or absolute value) of the complex shear modulus.

By substituting Eqs. (3) and (4) into Eq. (5), the following equation can be obtained:

$$G^* = \frac{H}{I_p} \frac{T_0 \ \exp[j\omega t]}{\alpha_0 \ \exp[j(\omega t - \varphi)]} \tag{6}$$

where $I_p = \frac{\pi R^4}{2}$ is the polar moment of inertia of the circular section.

Fig. 4 shows a typical example of the evolution of the norm of the complex shear modulus $|G^*|$ as a function of the number of cycles. During a fatigue test, three phases can be identified [24,25]. The first phase (or adaption phase), consisting of a rapid decrease of the complex modulus, is not attributable to fatigue but is caused by bulk reversible phenomena (e.g., self-heating, thixotropy). The second phase (or quasi-stationary phase) is associated with a quasi-linear decrease of the complex modulus, during which the initiation and propagation of micro-cracks within the specimen occur. In the third phase (or failure phase), irreversible phenomena (e.g., fatigue damage) start and a rapid decrease of the complex modulus begins. During this phase, macrocracks appear and propagate within the specimen, generating a not homogeneous distribution of stresses and strains. These three phases are not separated by a clear border but by a smooth transition zone.

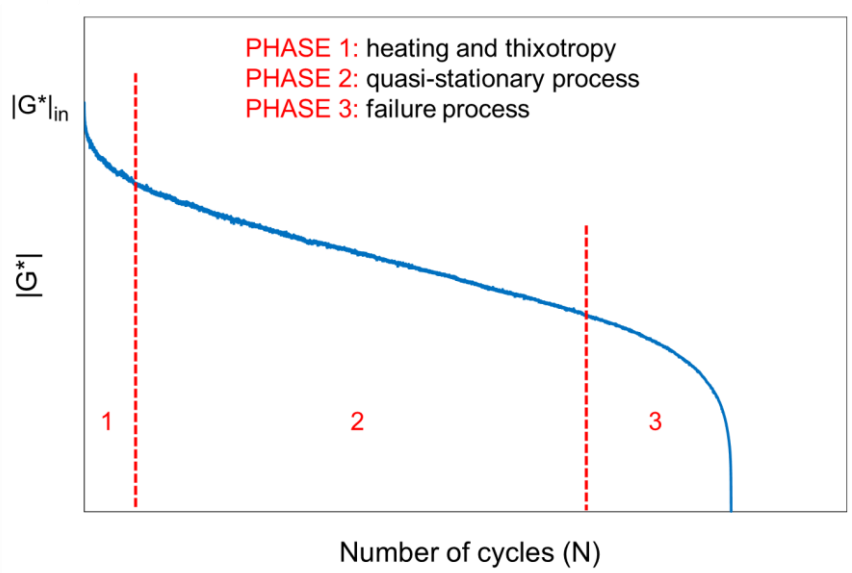

Fig. 4. Evolution of the norm of the complex shear modulus as a function of the number of cycles.

4.2 Double-layered specimens

The complex shear modulus G^* can be calculated with Eq. (6) only when single-layered systems are considered, whereas for double-layered cylindrical specimens the presence of the interface increases the complexity of the data analysis.

Specifically, when double-layered specimens are tested, G^* can be considered as an apparent modulus that takes into account the contribution of the two-layer asphalt concrete as well as the interlayer, assumed as a layer at the interface of appropriate thickness. Hence, the total height of the specimen (H) becomes equal to the sum of the heights of the lower layer (H_1), the upper layer (H_2) and the interlayer (H_i) (Fig. 5.a). Analogously, the amplitude of the torsional rotation angle α_0 comprises the torsional rotation angle of the asphalt mixture that characterises the lower and the upper layers plus the torsional rotation angle of the interlayer.

Since the fracture usually occurs in correspondence of the interface [23], it can be assumed that the shear strain of the interlayer γ_i and the interlayer complex shear modulus G_i^* are strictly linked to the specimen failure. Then, these two parameters were analytically determined in order to evaluate their evolution until failure.

In the following equations, the parameters obtained during the double-layered shear-torque fatigue tests and referred to the overall response of the specimen are named with the subscript "*bulk*", the parameters referred to the two layers in asphalt concrete are named with the subscript "*AC*" and the parameters referred to the interlayer are named with the subscript "*i*".

It can be assumed that the general trend of the maximum shear strain γ_{bulk} (i.e., γ_{max}), obtained during the double-layered test and denoted with a black dotted line in Fig. 5.b, can be schematically represented by the contribution of the shear strain of the asphalt concrete γ_{AC} (red dashed lines) and by the contribution of the interlayer shear strain γ_i (blue dashed line).

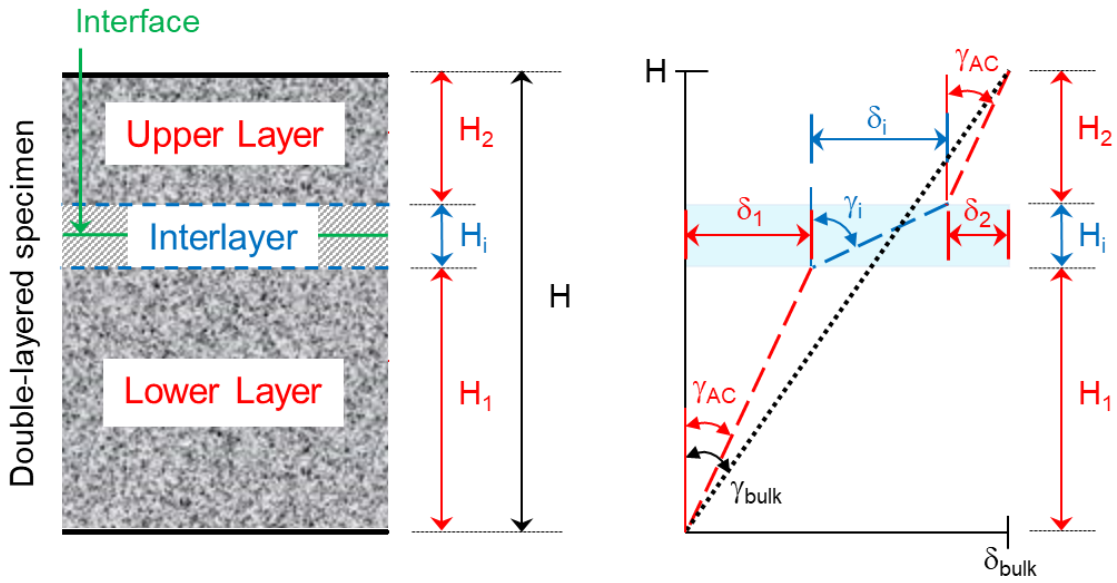

(a) (b)

Fig. 5. (a) Cross-section of a double-layered specimen and (b) plane representation of the shear strain interpretation (the figure is not drawn to scale).

Based on this assumption, it is possible to separate the different contributions to the shear strain.

Specifically, the value of the interlayer shear strain γ_i can be calculated as follows:

$$\gamma_i = \frac{\delta_i}{H_i} \tag{7}$$

where δ_i can be obtained by the following equation:

$$\delta_i = \delta_{bulk} - (\delta_1 + \delta_2) \tag{8}$$

Assuming that both layers are prepared with the same asphalt concrete, it can be considered that $\delta_1 = \gamma_{AC} \cdot H_1$ and $\delta_2 = \gamma_{AC} \cdot H_2$, leading the following equation:

$$\delta_i = \delta_{bulk} - \gamma_{AC} \cdot (H_1 + H_2) = \delta_{bulk} - \gamma_{AC} \cdot (H - H_i) \tag{9}$$

The shear strain of the asphalt concrete γ_{AC} can be calculated from the norm of the complex shear modulus $|G^*_{AC}|$, as follows:

$$\gamma_{AC} = \frac{\tau_{max,0}}{|G^*_{AC}|} \tag{10}$$

Considering that $\delta_{bulk} = R\alpha_0$, the substitution of Eqs. (9) and (10) in Eq. (7), allows to obtain:

$$\gamma_i = \frac{R\alpha_0 - \frac{\tau_{max,0}}{|G_{AC}^*|} \cdot (H - H_i)}{H_i} \tag{11}$$

199 Since the interlayer complex shear modulus G_i^* is expressed by the following equation:

$$G_i^* = \frac{\tau_{max,0}\ \exp[\mathrm{j}\omega t]}{\gamma_i \exp[\mathrm{j}(\omega t - \varphi)]} \tag{12}$$

200 its norm can be calculated, by using Eq. (11), as follows:

$$|G_i^*| = \frac{\tau_{max,0}}{\gamma_i} = \frac{\tau_{max,0} \cdot H_i}{R\alpha_0 - \frac{\tau_{max,0}}{|G_{AC}^*|} \cdot (H - H_i)} \tag{13}$$

201 Thus, the determination of the norm of the interlayer complex shear modulus $|G_i^*|$ is subjected to
202 the knowledge of the interlayer thickness H_i and of the norm of the complex shear modulus of
203 the asphalt concrete $|G_{AC}^*|$. The influence of both parameters ($|G_{AC}^*|$ and H_i) on the application of
204 Eq. (13) are studied in depth in Section 6.

205 **5. Experimental investigation**

206 **5.1 Materials and specimen preparation**

207 The asphalt concrete (AC) used for this study was a dense-graded mixture for surface courses
208 with 12.5 mm nominal maximum aggregate size (Fig. 6). The AC was prepared with a polymer-
209 modified bitumen (PMB) classified as 45/80-65 (EN 12591 [26]) and dosed at 5.5% by aggregate
210 mass.

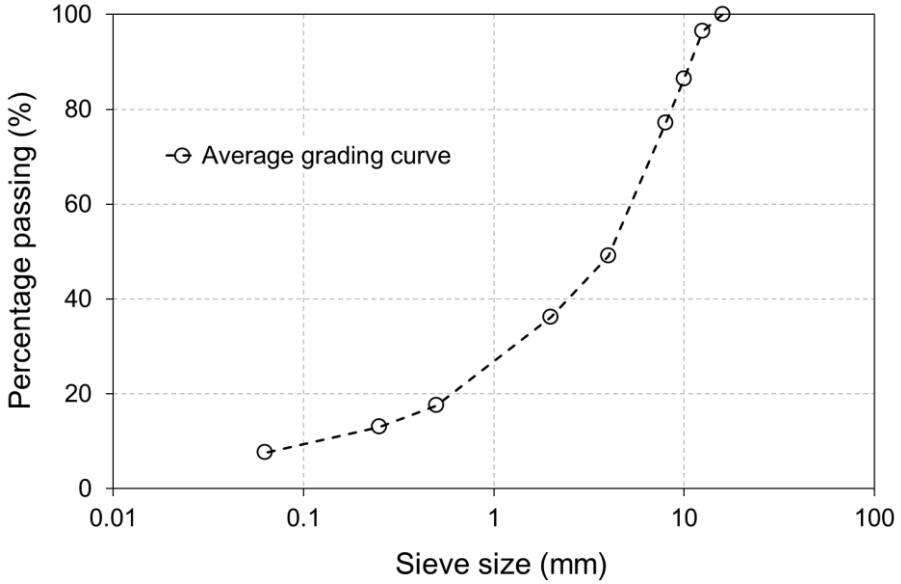

Fig. 6. Aggregate grading curve of the AC mixture.

The AC was compacted in the laboratory by means of a steel roller compactor (EN 12697-33 [27]), manufacturing three slabs (305 × 305 × 100 mm^3): one single-layered, named as A, and two double-layered, named as B and C. The slab A had a thickness of 100 mm, whereas the lower and the upper layers of slabs B and C had a thickness of 60 mm and 40 mm, respectively. No tack-coat was spread at the interface. All the layers were characterised by the same target air voids content (5%), to allow a reliable comparison in terms of interface performance.

Five cylindrical specimens (with a nominal diameter D = 100 mm) were cored from each slab (Fig. 7). Once cored, the upper and the lower parts of each specimen were sawed (about 10 mm) and, subsequently, trimmed with an abrasive disc circular saw in order to provide a ridge-free surface and to ensure parallel alignment of the edges of the specimen (Fig. 8). Only one cylindrical specimen without interface (obtained from slab A) and ten double-layered specimens (obtained from slabs B and C) were tested and analysed in the second and third phase of this investigation.

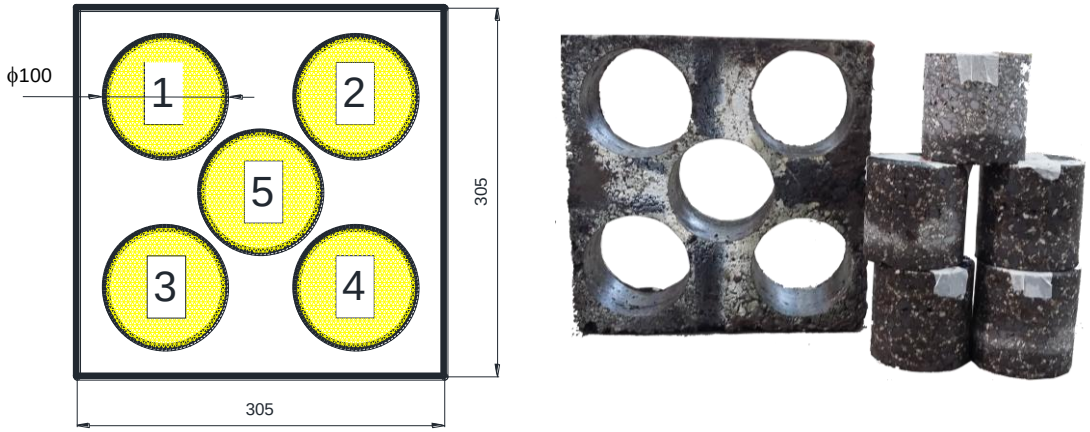

Fig. 7. Cylindrical specimens cored from the slabs.

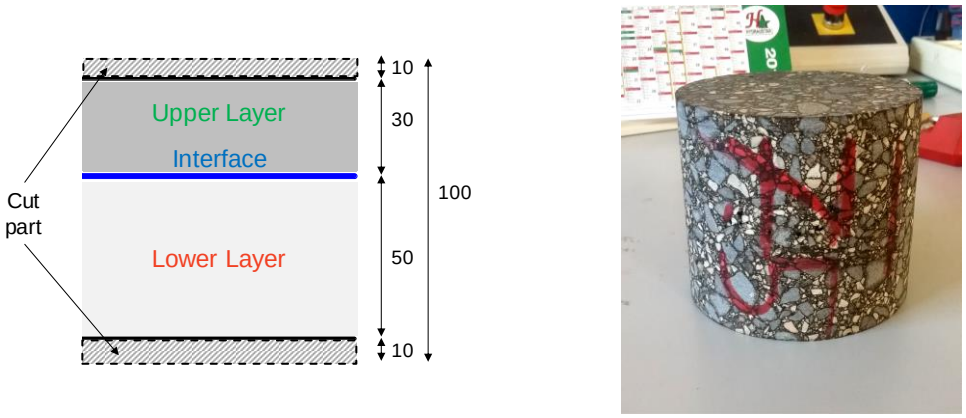

Fig. 8. Sawed and trimmed cylindrical specimens of slabs B and C.

5.2 Laboratory program

All the shear-torque fatigue tests were performed according to the procedure described in Section 3. Constant torque amplitudes (T_0) ranging from 70 to 100 Nm were applied during the investigation, according to a preliminary study which showed that these stress levels guarantee a proper number of cycles before failure.

For the preliminary validation of the model, shear-torque fatigue tests were performed on both one specimen of slab A (without interface) and one specimen of slab C (with interface), applying a torque amplitude T_0 equal to 80 Nm.

Finally, in order to correctly characterise the fatigue interlayer behaviour through the determination of the fatigue curve, the testing program shown in Table 1 was carried out. One

different level of torque amplitude was applied to each specimen, by stopping the test when the complete fracture of the specimen was obtained (i.e., the separation between the two layers).

Each specimen was named by means of an identification code (ID) that indicates the slab, the coring position (Fig. 7) and the applied torque amplitude; for example, A_2_80 represents the test on the specimen cored in the slab A, in the position #2, performed with a torque amplitude equal to 80 Nm.

Table 1. Experimental program of the third phase.

Slab	Specimen position #	Temperature °C	Frequency Hz	Torque amplitude T_0 Nm	Specimen ID
B	1	20	10	100	B_1_100
	2			95	B_2_95
	5			85	B_5_85
C	1	20	10	70	C_1_70
	2			85	C_2_85
	3			75	C_3_75
	4			80	C_4_80
	5			90	C_5_90

6. Preliminary validation of the model

The values of the norm of the complex shear modulus of A_2_80 (without interface) and C_4_80 (with interface) are shown in Fig. 9, as a function of the number of loading cycles.

Since the specimens were characterised by an analogous bulk density (about 2.42 g/cm^3) and by the same torque amplitude (T_0 = 80 Nm), Fig. 9 provides evidence that the interface represents a weakness zone, leading to early failure compared to the specimen without interface. Indeed, specimen C_4_80 failed after about 143,000 cycles with an evolution of $|G^*|$ showing the three phases of the decay law seen in Fig. 4, whereas the specimen A_2_80 did not fail even after 8,500,000 cycles. Due to the excessive testing time, the A_2_80 test was stopped when the decrease of the norm of the complex shear modulus was approximately 58%, before reaching the failure condition. For this reason, the first and the second phase of the decay law can be identified, whereas the third phase cannot be seen.

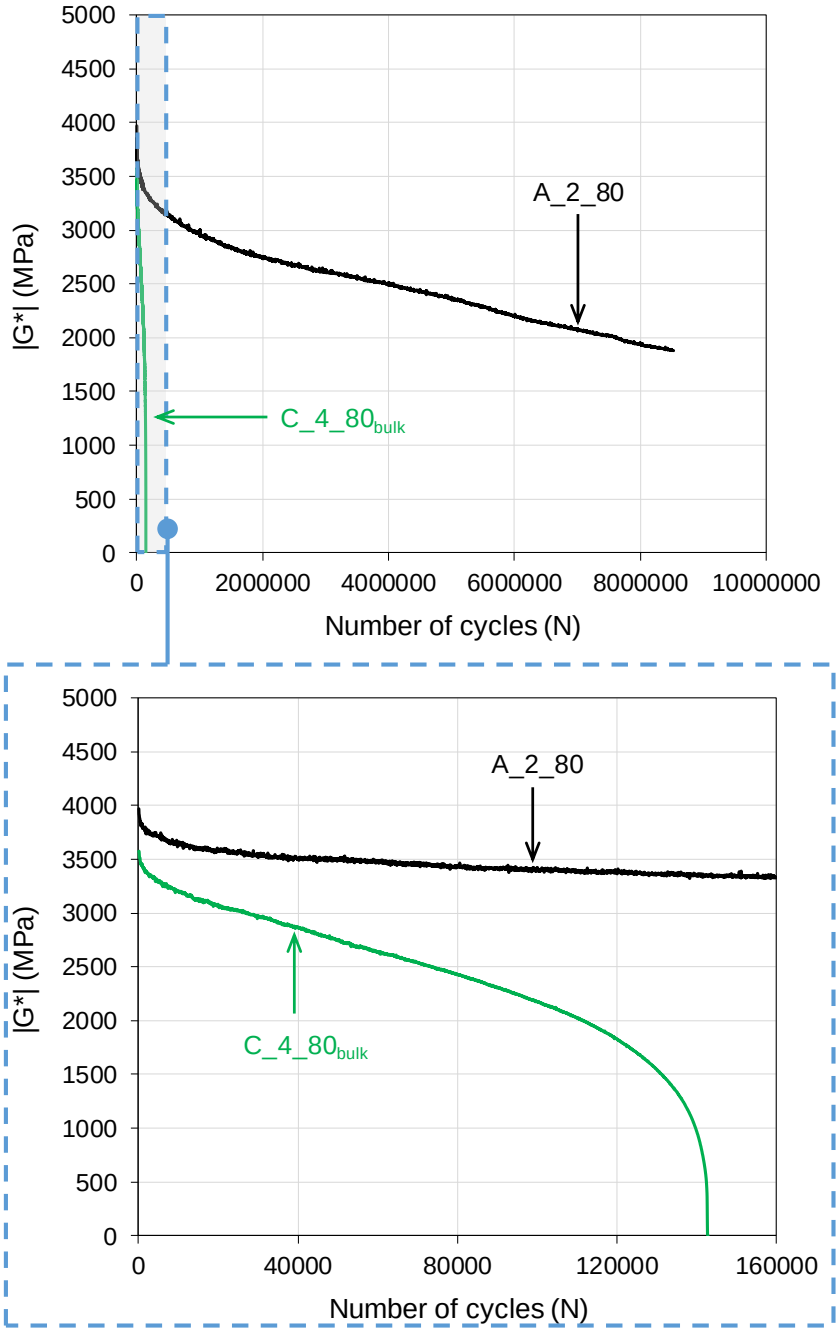

Fig. 9. Evolution of $|G^*|$ for specimens A_2_80 and C_4_80$_{bulk}$ during shear-torque fatigue test.

The remarkable difference just observed between the single-layered and the double-layered specimen confirms the assumption that the interlayer shear strain γ_i controls the failure of the latter. Thus, the effect of the presence of the interface on the response of double-layered systems under shear-torque fatigue loading was assessed by considering the interlayer complex shear modulus $|G_i^*|$ of the specimen C_4_80, determined according to Eq. (13). However, as above-

mentioned, a proper estimation of the norm of the complex shear modulus $|G^*_{AC}|$ and of the interlayer thickness H_i is fundamental for a correct evaluation of $|G^*_i|$. In the following observations, the variation of each of the two parameters was considered separately.

As regards the first parameter, it is necessary to determine if $|G^*_{AC}|$ can be assumed constant during the whole double-layered specimen test or if it must be considered progressively reduced. Indeed, during the test, $|G^*_{AC}|$ decreases due to the specimen damaging and it is important to understand the influence of this reduction on the $|G^*_i|$ determination. To this end, both a constant value and a progressive reduction law of $|G^*_{AC}|$ were considered in Eq. (13), by fixing a realistic interlayer thickness of 15 mm, according to Ragni et al. findings [23].

As far as the constant value law of $|G^*_{AC}|$ is concerned, it can be assumed that the double-layered specimen initially reacts as a single-layered system, so that the $|G^*_{AC}|$ can be considered equal to the $|G^*|_{bulk}$ of the C_4_80 in the first loading cycles (when the specimen is not yet damaged), allowing the determination of $|G^*_i|_{const}$ by means of Eq. (13).

On the other hand, the progressive reduction of $|G^*_{AC}|$ was evaluated through the study of the behaviour of the single-layered specimen A_2_80. Specifically, Fig. 9 clearly shows that, during the testing time of C_4_80 (about 143,000 cycles), also $|G^*|$ of A_2_80 is subjected to a gradual reduction, leading to consider that also the AC outside the interlayer likely suffers some damage during the C_4_80 shear-torque fatigue loading. Thus, cycle by cycle, the decay law of $|G^*|$ of A_2_80 was deduced and used for obtaining the decay law of $|G^*_{AC}|$ of C_4_80 (named $|G^*_{AC}|_{red}$). This law was introduced into Eq. (13), by allowing the calculation of $|G^*_i|_{red}$ of C_4_80 in correspondence of each cycle.

Finally, in order to allow an easier comparison, the values assumed by $|G^*_i|_{const}$ and $|G^*_i|_{red}$ at the n^{th} cycle were normalised with respect to their initial values and plotted as a function of the number of loading cycles, as shown in Fig. 10 (C_4_80$_{i\text{-}const}$ and C_4_80$_{i\text{-}red}$, respectively). In the same figure, also the evolution of the normalised moduli of the specimen without interface, A_2_80, and of the double-layered specimen C_4_80$_{bulk}$ are shown.

The differences observed between C_4_80$_{i\text{-}const}$ and C_4_80$_{i\text{-}red}$ in the greatest part of the test are obviously due to the fact that in the calculation of C_4_80$_{i\text{-}const}$ it is assumed that all the damage is immediately localised at the interface, whereas, for C_4_80$_{i\text{-}red}$, part of the damage affects also the AC outside the interlayer. However, in the proximity of the end of the test, the two interlayer moduli ($|G_i^*|_{const}$ and $|G_i^*|_{red}$) become very similar and thus, at this stage, the effect of the reduction of $|G_{AC}^*|$ plays a minor role in the damage trend of $|G_i^*|$. Thus, since it has been shown by Ragni et al. [23] that the "effective" damage at the interface occurs in the proximity of the end of the test, the assumption of considering a constant value for $|G_{AC}^*|$ can be considered valid without committing significant errors.

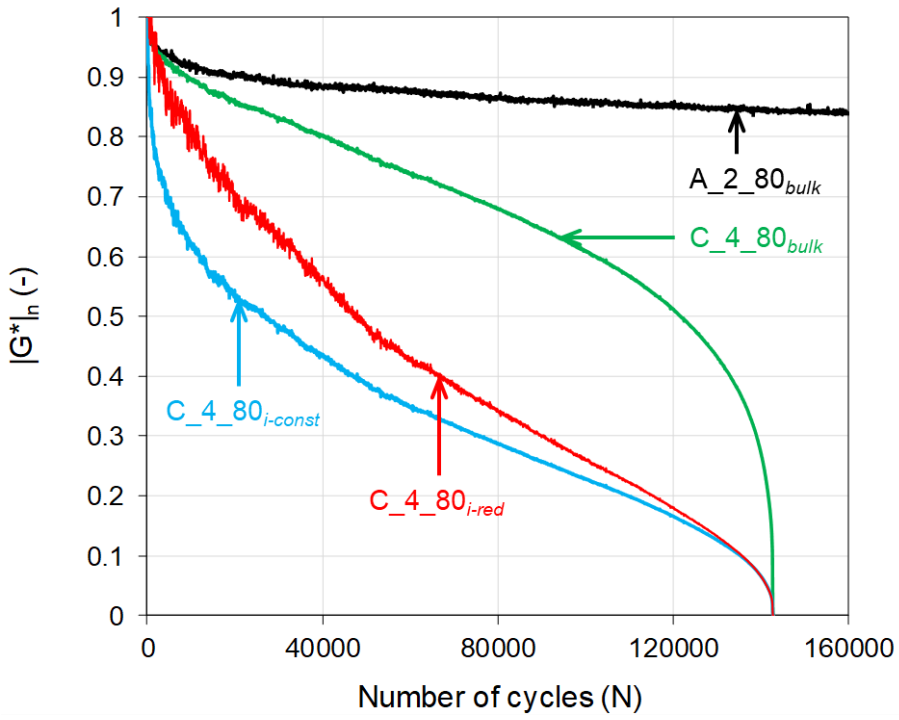

Fig. 10. Evolution of $|G^*|_n$ for specimens A_2_80 and C_4_80$_{bulk}$ during shear-torque fatigue test.

The second aspect, that should be taken into account, is the selection of the proper value for the interlayer thickness H_i. In this regard, Ktari et al. [28] performed monotonic tensile tests on double-layered asphalt specimens and used the Digital Image Correlation (DIC) technique to identify the interphase thickness (i.e., interlayer thickness H_i). They found out that the H_i can be assumed equal to 3 mm. In this study, a range of variation from 3 to 21 mm, with a step of 2 mm,

was considered for this parameter (H_i), by assuming a constant value for $|G^*_{AC}|$, equal to $|G^*|_{bulk}$ of C_4_80 in the first loading cycles (see above).

Fig. 11 presents $|G^*_i|$ (in blue), obtained with different values of H_i, as a function of the number of loading cycles, as well as the comparison with the corresponding $|G^*|_{bulk}$ (named as C_4_80$_{bulk}$). Fig. 11 clearly shows that $|G^*_i|$ curves are characterised by the typical three phases of fatigue tests. At the beginning, $|G^*_i|$ decreases drastically and then decreases quite steadily until approaching the end of the test, when a sudden reduction of the interlayer modulus occurs. It can be observed that a sudden decrease in the initial value of $|G^*_i|$ occurs for low H_i values (i.e., less than 11 mm), indicating that $|G^*_i|$ is markedly affected by the value of the interlayer thickness H_i. The higher the H_i value, the closer $|G^*_i|$ to the behaviour of $|G^*|_{bulk}$ (C_4_80$_{bulk}$).

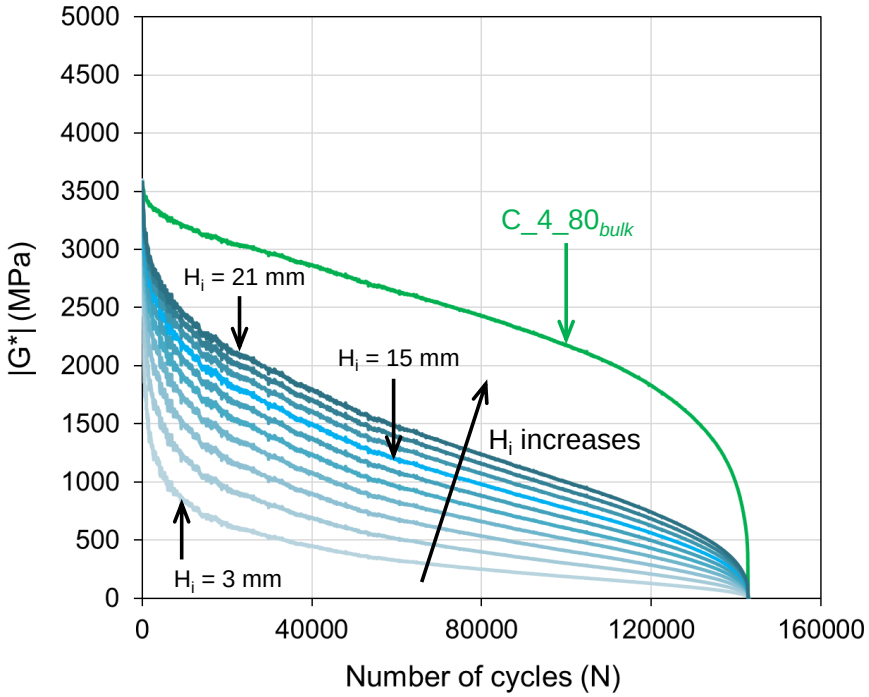

Fig. 11. Evolution of $|G^*|_{bulk}$ and $|G^*_i|$ for specimen C_4_80$_{bulk}$ during shear-torque fatigue test.

Since the applied torque induces a mechanical response within the material in the form of shear strain γ and the increase in the strain is usually due to damage accumulation in the material, it is interesting to evaluate the influence of the interlayer thickness H_i on this parameter. In Fig. 12, the shear strain of the bulk system γ_{bulk} and the interlayer shear strain γ_i of the specimen C_4_80

(in blue) for different values of H_i, are reported. The shear strain of the bulk system γ_{bulk} shows a two-phase process consisting of an almost constant trend until the proximity of the end of the test is reached when a sharp increase occurs. It is therefore clear that the double-layered specimen absorbs the shear-torque fatigue loading by producing very low shear deformations for the greatest part of the test duration. On the contrary, γ_i shows three distinct phases, whose evolution strongly depends on the value of H_i. The higher the value of H_i, the closer γ_i to the behaviour of γ_{bulk}. Specifically, changes in shear strain appear to be more noticeable assuming an interlayer thickness less than 11 mm. These outcomes suggest that H_i appears to be the variable which plays the most important role in the interlayer characterisation. For this reason, further research focused on the accurate identification of H_i (for example, by utilising digital image correlation technique) can considerably help in the development of a more precise evaluation of the interlayer behaviour. Nevertheless, an interlayer thickness H_i equal to 15 mm was assumed in the following discussion, according to Ragni et al. [23] findings.

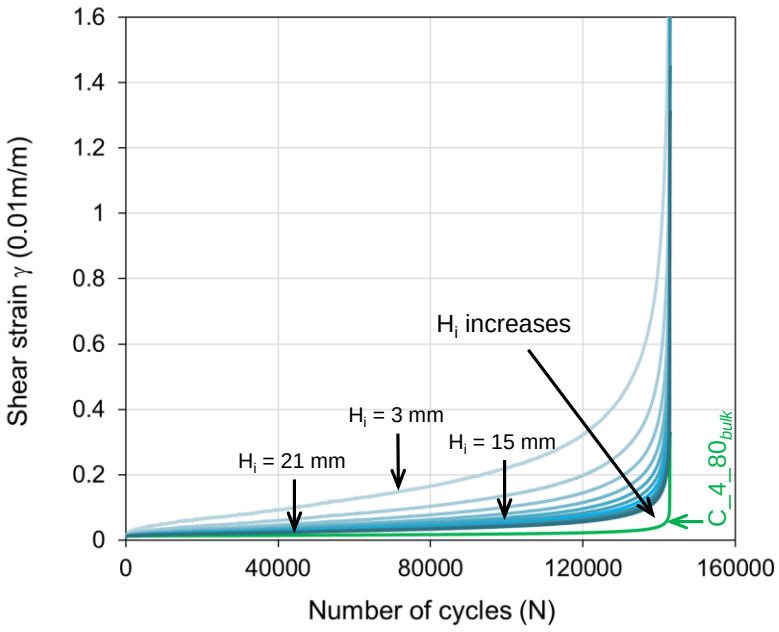

Fig. 12. Evolution of γ_{bulk} and γ_i for specimen C_4_80$_{bulk}$ during shear-torque fatigue test.

7. Interlayer shear fatigue curve

7.1 Fatigue failure criterion

A proper failure criterion should predict the fatigue life of the material and capture the failure of the specimen accurately (i.e., in this case, the formation of macro-cracks at the interface). In this regard, Ragni et al. [23] showed that, for shear-torque fatigue tests performed on double-layered specimens, the classical fatigue failure criterion (which defines failure as the point at which the stiffness modulus value reduces to 50% of its initial value) seems to provide an inaccurate estimation of the number of cycle to failure (N_f) since it is not able to quantify the damage mechanisms that occur within double-layered specimens. In the same study [23], the authors suggested that a failure criterion characterised by a 70% reduction of $|G^*|_{bulk}$ seems to better describe the material behaviour under shear-torque fatigue loading.

As an example, Fig. 13.a through Fig. 13.d present the criterion of the 70% reduction of $|G^*|_{bulk}$ applied to four test results in this study. These graphs suggest that the number of cycles to failure (N_f) determined based on this failure criterion correspond to a reduction of the interlayer complex shear modulus $|G_i^*|$ approximately equal to 90%, that is $|G^*|_n$ = 0.1. Consequently, rather than to use the 70% reduction of $|G^*|_{bulk}$, the 90% reduction of the initial value of the interlayer complex shear modulus $|G_i^*|$ can be adopted as a failure criterion for shear-torque fatigue test carried out on double-layered asphalt specimens. Moreover, it can also be noted that the evolution of $|G^*|_n$ for the specimen B_5_85 (Fig.13.b) significantly differs from that of the other specimens. An analogous trend was also found for the specimen C_5_90, not reported in Fig. 13. This behaviour could be due to the crack pattern at the interface obtained for these two specimens, as described in the following section.

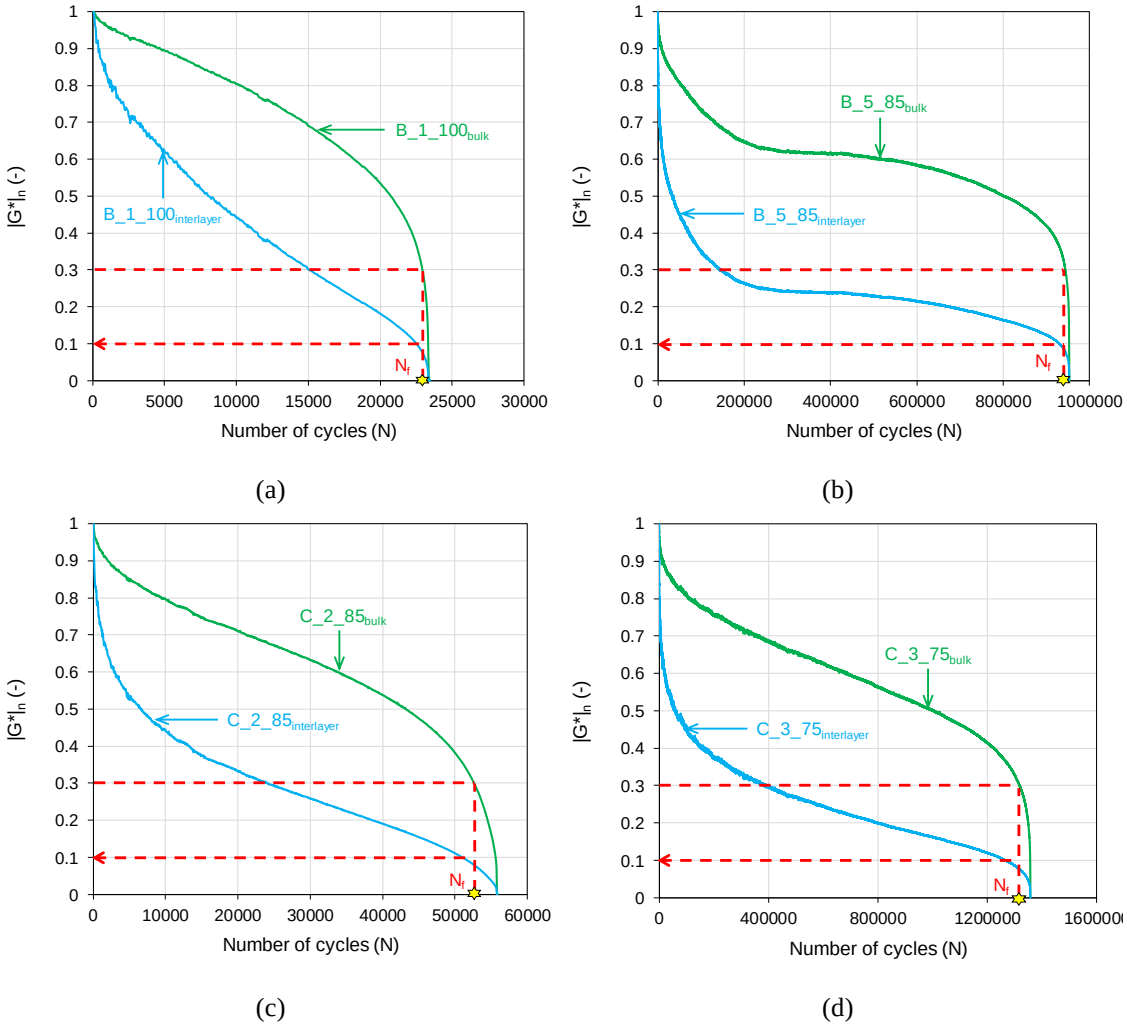

Fig. 13. Evolution of $|G^*|_n$ during shear-torque fatigue test and fatigue failure criterion: (a) B_1_100; (b) B_5_85; (c) C_2_85; (d) C_3_75.

7.2 Fatigue curve

In Fig. 14, the interlayer shear fatigue curve of the specimens cored from slabs B and C is plotted in a log-log plane. Such analysis was based on a power-law relationship between the amplitude of the applied shear stress $\tau_{max,0}$ and the number of loading cycles to failure N_f, recorded in correspondence of the 90% reduction of the initial value of $|G_i^*|$, using the following equation:

$$\tau_{max,0} = a \cdot {N_f}^{-b} \tag{14}$$

where the parameters a and b are regression coefficients and usually depend on both material and testing temperature. Specifically, b represents the slope of the linear regression which is obtained in a log-log plane.

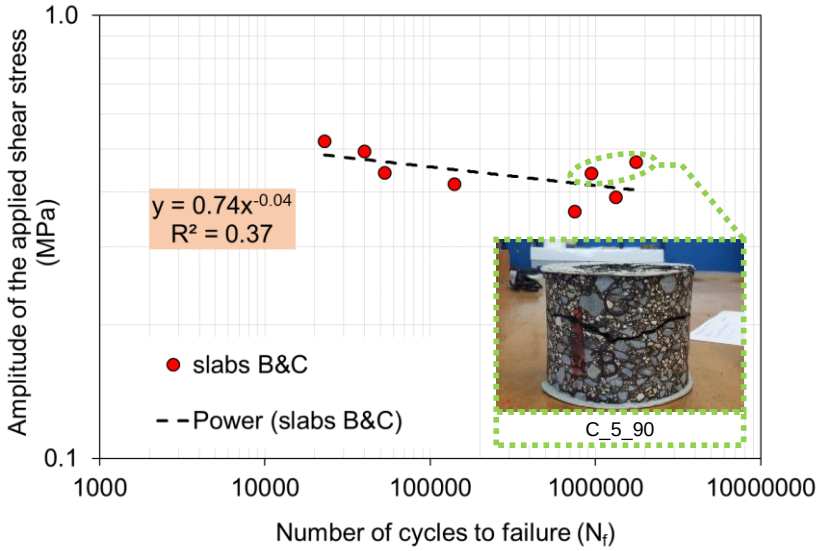

Fig. 14. Interlayer shear fatigue curve in terms of the amplitude of the applied shear stress as a function of the number of cycles to failure.

Fig. 14 shows that, in general, as the level of shear stress (i.e., torque) decreases, the shear fatigue life of the bituminous material increases even if the correlation between the obtained data is not good ($R^2 = 0.37$). This can be due to the fact that the two data points circled in green, do not follow the general trend as they provide higher values of N_f for higher values of $\tau_{max,0}$. Looking for the reason for this behaviour, it was observed that, in both cases (specimens B_5_85 and C_5_90), the crack pattern at the interface was irregular (see the box in Fig. 14), contrarily to what happened for all the other specimens, for which the fracture occurred exactly at the interface (Fig. 15). This finding corroborates what observed in Fig. 13, where different evolution of $|G^*|_n$ were found for B_5_85 (as well as C_5_90) with respect to the others. As above-mentioned, this different behaviour can be due to the different crack pattern at the interface observed for these two specimens, suggesting that a visual failure inspection of the specimens is essential for developing a correct interlayer fatigue characterisation. Moreover, it was noticed that both these specimens (B_5_85 and C_5_90) were cored at the centre of the slabs (i.e., position #5 of Fig. 7), where a better interlocking between the two bituminous layers in contact could be achieved due to the not homogeneous compaction process performed by the roller compactor (i.e., higher compaction energy is expected in the centre of the slab) [29,30]. However, it should be mentioned

that, among the laboratory methods used to fabricate laboratory specimens, the roller compactor provides the best correlation with field cores in terms of both internal aggregate structure and mechanical properties [31-33].

Fig. 15. Failure mechanisms of the specimens at the border of the slab.

The updated interlayer shear fatigue curve is reported in Fig. 16, in which the specimens cored in position #5 (empty dots) were not considered. In this case, the good correlation coefficient ($R^2 = 0.85$) clearly indicates that the coring position is relevant, at least for shear-torque fatigue tests.

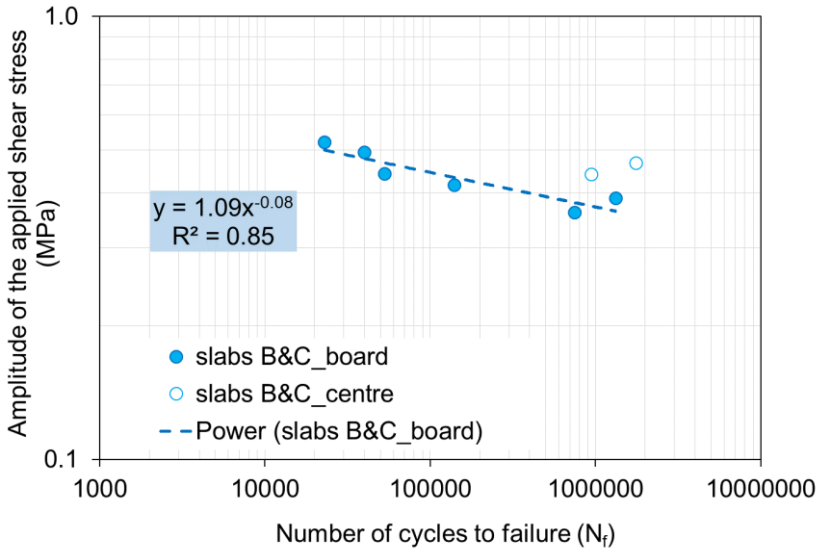

Fig. 16. Interlayer shear fatigue curve of the border specimens in terms of the amplitude of the applied shear stress as a function of the number of cycles to failure.

It can be concluded that the fatigue process of double-layered specimens is a complex phenomenon due to a twofold factor: the heterogeneous nature of the bituminous material and the

presence of a weakness zone (i.e., interlayer). Other viscoelastic phenomena occur during fatigue tests (e.g., self-heating, thixotropy, non-linearity) but have not been taken into account in this study.

8. Conclusions

This paper focuses on the evaluation of the fatigue behaviour of pavement bituminous interlayers subjected to shear-torque fatigue tests. A preliminary experimental investigation was carried out on single- and double-layered specimens to investigate the influence of the interface on shear-torque fatigue properties. Based on these preliminary finding, a model describing the evolution of the interlayer damage and a new fatigue failure criterion were proposed in order to correctly identify the material behaviour at the interface and to overcome the classical damage approach. The following main conclusions can be drawn:

- the presence of the interface represents a weakness zone in the double-layered specimen and, therefore, it noticeably influences the shear fatigue performance;
- the norm of the interlayer complex shear modulus and the norm of the complex shear modulus decrease as the number of loading cycles increases, indicating that the first can be a good indicator of the damage of the specimen interface;
- the proposed model describes the evolution of the interlayer damage of double-layered specimens under shear-torque fatigue tests through the analysis of the variation of the norm of the interlayer complex shear modulus. Preliminary validation of the model showed that it adequately characterises the evolution of the interlayer properties during cyclic torque loading even if further refinements to the model are needed;
- a new fatigue failure criterion, which seems to better correspond to the mechanisms of failure that occurred at the interface of double-layered specimens, was proposed for shear-torque fatigue test;

- a comparison between specimens cored at the centre and at the border of the compacted slabs seems to show the existence of non-uniform compaction which is reflected in a dissimilar shear fatigue life. This result must be confirmed by future experimentation.

Summarising, this study suggests that the proposed testing method and analysis can effectively provide a noticeable help for the understanding of shear-torque fatigue phenomena at the interface of double-layered asphalt concrete specimens. The work herein represents a fundamental basis for future developments required to confirm the theoretical assumptions. Further experiments will be carried out by broadening the tested materials (layers composed of different asphalt mixtures) to assess the reliability and accuracy of the model as well as to validate the proposed fatigue failure criterion.

Declaration of competing interest

The authors declare that they have no known competing financial interests or personal relationships that could have appeared to influence the work reported in this paper.

References

[1] J. Uzan, M. Livneh, Y. Eshed, Investigation of adhesion properties between asphalt concrete layers, J. Assoc. Asphalt Paving Technol., 1978, 47, 495–521.

[2] M.Y. Shahin, K. Kirchner, E. Blackmon, Analysis of asphalt concrete layer slippage and its effect on pavement performance and rehabilitation design, In: Proceedings of 6th International Conference Structural Design of Asphalt Pavements, July 13-17, 1987, 958–964, Ann Arbor.

[3] H. Al Nageim, B. Al Hakim, Bonding conditions between pavement layers and their influence on pavement layers moduli and remaining life, In: Proceeding of 3rd European Symposium on Performance and Durability of Bituminous Materials and Hydraulic Stabilised Composites, April 8-9, 1999, Leeds.

448 [4] S. Romanoschi, J. Metcalf, Characterization of asphalt concrete layer interfaces, Transp.
449 Res. Rec.: J. Transp. Res. Board, 2001, 1778(1), 132–139, https://doi.org/10.3141%2F1778-16.

450 [5] F. Canestrari, G. Ferrotti, X. Lu, A. Millien, M.N. Partl, C. Petit, A. Phelipot-Mardelé, H.
451 Piber, C. Raab, Mechanical testing of interlayer bonding in asphalt pavements, In: Partl M. et al.
452 (eds) Advances in Interlaboratory Testing and Evaluation of Bituminous Materials, RILEM State-
453 of-the-Art Reports, 2013, 9, 303–360, Springer, Dordrecht, https://doi.org/10.1007/978-94-007-
454 5104-0_6.

455 [6] C. Petit, A. Chabot, A. Destrée, C. Raab, Recommendation of RILEM TC 241-MCD on
456 interface debonding testing in pavements, Mater. Struct., 2018, 51(4), 96,
457 https://doi.org/10.1617/s11527-018-1223-y.

458 [7] F. Canestrari, E. Santagata, Temperature effects on the shear behaviour of tack coat
459 emulsions used in flexible pavements, Int. J. Pavement Eng., 2005, 6(1), 39–46,
460 https://doi.org/10.1080/10298430500068720.

461 [8] F. Canestrari, G. Ferrotti, M.N. Partl, E. Santagata, Advanced testing and characterization
462 of interlayer shear resistance, Transp. Res. Rec.: J. Transp. Res. Board, 2005, 1929(1), 69–78,
463 https://doi.org/10.1177/0361198105192900109.

464 [9] F.A. Santagata, M.N. Partl, G. Ferrotti, F. Canestrari, A. Flisch, Layer characteristics
465 affecting interlayer shear resistance in flexible pavements, J. Assoc. Asphalt Paving Technol.,
466 2008, 77, 221–256.

467 [10] C. Raab, M.N. Partl, Interlayer bonding of binder, base and subbase layers of asphalt
468 pavements: long-term performance, Constr. Build. Mater., 2009, 23(8), 2926–2931,
469 https://doi.org/10.1016/j.conbuildmat.2009.02.025.

470 [11] R. Ktari, F. Fouchal, A. Millien, C. Petit, Surface roughness: a key parameter in pavement
471 interface design, Eur. J. Environ. Civ. Eng., 2017, 21(sup1), 27–42,
472 https://doi.org/10.1080/19648189.2017.1304284.

[12] C. Raab, M.N. Partl, A.O. Abd El Halim, Evaluation of interlayer shear bond devices for asphalt pavements, Balt. J. Road Bridge E., 2009, 4(4), 186–195, https://doi.org/10.3846/1822-427x.2009.4.186-195.

[13] F. Canestrari, G. Ferrotti, A. Graziani, Shear failure characterization of time–temperature sensitive interfaces, Mech. Time-Depend. Mater., 2016, 20, 405–419, https://doi.org/10.1007/s11043-016-9299-7.

[14] A. Graziani, F. Canestrari, F. Cardone, G. Ferrotti, Time–temperature superposition principle for interlayer shear strength of bituminous pavements, Road Mater. Pavement Des., 2017, 18(sup2), 12–25, https://doi.org/10.1080/14680629.2017.1304247.

[15] D. Ragni, A. Graziani, F. Canestrari, Cyclic interlayer testing in bituminous pavements, In: Proceedings of the 7th International Conference Bituminous Mixtures and Pavements (7ICONFBMP), June 12-14, 2019, Thessaloniki, https://doi.org/10.1201/9781351063265-31.

[16] M. Diakhaté, A. Millien, C. Petit, B. Phelipot-Mardelé, B. Pouteau, Experimental investigation of tack coat fatigue performance: towards an improved lifetime assessment of pavement structure interfaces, Constr. Build. Mater., 2011, 25(2), 1123–1133, https://doi.org/10.1016/j.conbuildmat.2010.06.064.

[17] A. Zofka, M. Maliszewski, A. Bernier, R. Josen, A. Vaitkus, R. Kleizienė, Advanced shear tester for evaluation of asphalt concrete under constant normal stiffness conditions, Road Mater. Pavement Des., 2015, 16(sup1), 187–210, https://doi.org/10.1080/14680629.2015.1029690.

[18] C. Raab, M.N. Partl, E. Fourquet, A.O. Abd El Halim, Static and cyclic evaluation of interlayer bonding, In: Proceedings of the 10th International Conference on the Bearing Capacity of Roads, Railways and Airfields (BCRRA 2017), June 28-30, 2017, 1511–1516, Athens, https://doi.org/10.1201/9781315100333-200.

[19] I. Isailović, M.P. Wistuba, Asphalt mixture layers' interface bonding properties under monotonic and cyclic loading, Constr. Build. Mater., 2018, 168, 590–597, https://doi.org/10.1016/j.conbuildmat.2018.02.149.

[20] A. D'Andrea, C. Tozzo, Dynamic tests on bituminous layers interface, Mater. Struct., 2016, 49, 917–928, https://doi.org/10.1617/s11527-015-0548-z.

[21] W. Song, X. Shu, B. Huang, M. Woods, Laboratory investigation of interlayer shear fatigue performance between open-graded friction course and underlying layer, Constr. Build. Mater., 2016, 115, 381–389, https://doi.org/10.1016/j.conbuildmat.2016.04.060.

[22] A.C. Collop, M.H. Sutanto, G.D. Airey, R.C. Elliot, Development of an automatic torque test to measure the shear bond strength between asphalt, Constr. Build. Mater., 2011, 25(2), 623–629, https://doi.org/10.1016/j.conbuildmat.2010.07.030.

[23] D. Ragni, M. Takarli, C. Petit, A. Graziani, F. Canestrari, Use of acoustic techniques to analyse interlayer shear-torque fatigue test in asphalt mixtures, Int. J. Fatigue, 2020, 131, 105356, https://doi.org/10.1016/j.ijfatigue.2019.105356.

[24] H. Di Benedetto, C. de La Roche, H. Baaj, A. Pronk, R. Lundström, Fatigue of bituminous mixtures, Mater. Struct., 2004, 37, 202–216, https://doi.org/10.1007/BF02481620.

[25] Q.T. Nguyen, H. Di Benedetto, C. Sauzéat, Determination of thermal properties of asphalt mixtures as another output from cyclic tension-compression test, Road Mater. Pavement Des., 2012, 13(1), 85–103, https://doi.org/10.1080/14680629.2011.644082.

[26] EN 12591, Bitumen and bituminous binders – Specifications for paving grade bitumens, 2009.

[27] EN 12697-33, Bituminous mixtures – Test methods for hot mix asphalt – Part 33: specimen prepared by roller compactor, 2007.

[28] R. Ktari, A. Millien, F. Fouchal, I.-O. Pop, C. Petit, Pavement interface damage behavior in tension monotonic loading, Constr. Build. Mater., 2016, 106, 430–442. https://doi.org/10.1016/j.conbuildmat.2015.12.020.

[29] E. Masad, B. Muhunthan, N. Shashidhar, T. Harman, Quantifying laboratory compaction effects on the internal structure of asphalt concrete, Transp. Res. Rec.: J. Transp. Res. Board, 1999, 1681(1), 179–185, https://doi.org/10.3141/1681-21.

[30] E.A. Hunter, G.D. Airey, A.C. Collop, Aggregate orientation and segregation in laboratory-compacted asphalt samples, Transp. Res. Rec.: J. Transp. Res. Board, 2004, 1891, 8–15, https://doi.org/10.3141/1891-02.

[31] G.D. Airey, A.C. Collop, Mechanical and structural assessment of laboratory- and field-compacted asphalt mixtures, Int. J. Pavement Eng., 2016, 17(1), 50–63, https://doi.org/10.1080/10298436.2014.925551.

[32] G.D. Airey, A.C. Collop, S. Zoorob, The influence of laboratory compaction methods on the performance of asphalt mixtures, Final Report, Engineering and Physical Science Research Council, 2005.

[33] V. Dubois, C. De La Roche, O. Burban, Influence of the compaction process on the air void homogeneity of asphalt mixtures samples, Constr. Build. Mater., 2010, 24(6), 885–897, https://doi.org/10.1016/j.conbuildmat.2009.12.004.